Magnetic circularly polarized $2p$ resonant photoemission of nickel

L. H. Tjeng, C. T. Chen, P. Rudolf, and G. Meigs

AT&T Bell Laboratories, 600 Mountain Avenue, Murray Hill, New Jersey 07974

G. van der Laan

Daresbury Laboratory, Warrington WA4 4AD, United Kingdom

B. T. Thole

Materials Science Center, University of Groningen, Nijenborgh 4, 9747 AG Groningen, The Netherlands

We report the observation of two resonance channels in the $2p$ resonant photoemission of ferromagnetic nickel using circularly polarized soft x rays. By identifying the local $3d^8$ and $3d^7$ configurations in the valence-band photoemission spectra, we are able to assign structures in $2p$ core-level-absorption and magnetic-circular-dichroism spectra to many-body $2p^5 3d^{10}$ and $2p^5 3d^9$ configurations as well as to a critical point in the band structure. The Ni data provide a critical test for theoretical models of x-ray absorption and magnetic-circular-dichroism spectroscopy of transition-metal magnetic materials. This work also demonstrates the unique possibilities provided by circularly polarized light for separating the Auger process from the resonant-photoemission process and unraveling the electronic structure.

Circularly polarized core-level photoabsorption and photoemission of magnetic systems have recently attracted much attention, both experimentally[1] and theoretically.[2-5] This type of spectroscopy has been demonstrated to provide valuable information on the electronic and magnetic structure of matter, and is expected to become, in the near future, a well established technique for studying magnetism and magnetic materials. The influence of the strong interplay between the band-structure and electron correlation effects on the x-ray-absorption (XAS) and magnetic-circular-dichroism (MCD) spectra of metallic magnetic transition metals, however, is still not well understood. In particular, a recent soft-x-ray MCD measurement, reporting absorption features near the $L_{2,3}(2p_{1/2,3/2} \to 3d)$ white lines of Ni, has provoked discussions on this issue.[3-5] Figure 1 reproduces these XAS and MCD spectra of Ni, showing the intense $L_{2,3}$ white lines, together with their fine structures. Interestingly, among these fine structures, the peaks A, A' observed in the XAS spectrum show nearly no MCD, while the peaks B, B', which are imperceptible in the XAS spectrum, appear as distinct shoulders in the MCD spectrum.[3]

A recent relativistic tight-binding band-structure calculation[3] has pointed out that although the independent particle picture can reproduce both the XAS and MCD intensity of the white lines and peaks A, A', it fails to explain the appearance of peaks B, B'. On the other hand, a configuration-interaction analysis,[4,5] based on the Anderson impurity model including atomic multiplet structure, is able to explain peaks B, B', but cannot account for the observed XAS intensity or the disappearance of the MCD in peaks A, A'. It is not clear how to interpret these XAS and MCD fine structures, and a clarification is required because of the implications for the theoretical modeling and, subsequently, for the calculated (near) ground-state properties such as the magnitude of local

moments and their interactions. In a band-structure calculation, for instance, local magnetic moments and MCD effects are due to the exchange splitting, while in the Anderson impurity model they originate from local atomic multiplet effects (which gives the Hund's rule for the ground state). This study on elemental Ni might be viewed as a critical test case for theories describing XAS and MCD spectroscopies of the technologically relevant class of transition-metal magnetic materials.

In this paper we report the unique use of magnetic-circular polarization in our resonant photoemission study
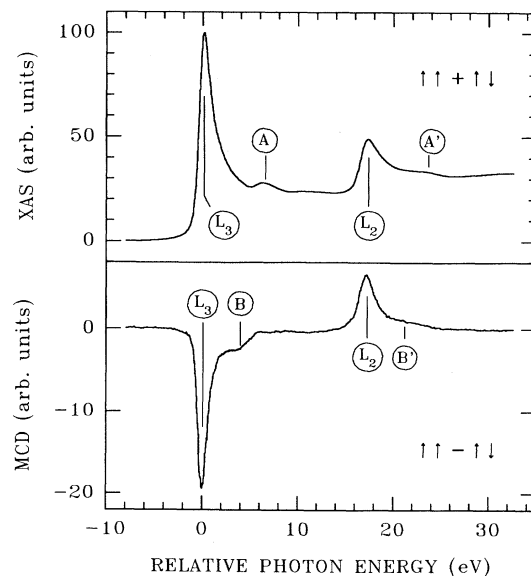

Fig. 1. $L_{2,3}$ edge x-ray-absorption spectra of Ni: total absorption (top) and magnetic-circular dichroism (bottom). Fine structures labeled A, A' and B, B' are discussed in the text.

on nickel with photon energies near the L_3 white line. The purpose of this paper is to identify the origin of the observed XAS and MCD fine structures; to appraise the different views on the relative importance of local correlation and transitional-symmetry effects in XAS and MCD spectra; and to demonstrate the capability of magnetic-circular polarization to separate the Auger process from the resonant-photoemission process and unravel the electronic structure of magnetic materials. The data show two deexcitation channels in the $2p$ resonant photoemission process, thereby identifying the local $2p^5 3d^{10}$ and $2p^5 3d^9$ configurations in the XAS and MCD spectra, and the $3d^8$ and $3d^7$ configurations in the valence-band photoemission spectra. Peaks, B, B' in the MCD spectrum can be assigned to local many-body effects, and a large portion of the intensity of peaks A, A' in the XAS spectrum can be attributed to a critical point in the band structure. Identification of these photoabsorption and photoemission final states would not be possible using unpolarized light, which underscores the value of magnetic circularly polarized spectroscopies.

The experiments were performed at the AT&T Bell Laboratories Dragon beamline at the National Synchrotron Light Source.[6] The beamline optical arrangement in the circular mode has been described previously.[6] The photoelectrons were detected with a hemispherical analyzer equipped with multichannel detection. The photon energy resolution and electron kinetic energy resolution were both set at 0.8 eV. The degree of circular polarization

was set at 77% to optimize the circular dichroism signal-to-noise ratio.[6] The measurements were carried out on a thin Ni film (≈ 10 monolayers) evaporated onto a clean and well ordered Cu(100) surface. A thin film was used instead of a bulk Ni sample because of the easier magnetization and less stray magnetic field. The XAS, MCD, Auger, $2p$ core-level, and ($2p$ resonant) valence-band photoemission spectra were all found to be identical to those of thicker Ni films and of bulk Ni. The 10-ML film thickness is sufficient to conceal all photoemission signal from the underlying Cu substrate. The light was at grazing incidence along the [010] surface plane direction and a remnant magnetic field was established in the Ni film along the same [010] surface direction by using an *in situ* pulsed electromagnet. The magnetic circular polarized photoemission spectra were obtained using the four possible combinations of light helicity (right/left) and sample magnetization direction (parallel/antiparallel to the light incidence) in order to exclude any systematic errors. The entire measurements took about two weeks; and, for every 24 h, a fresh Ni film was made to ensure sample surface cleanliness. The measurements were carried out at room temperature.

Figure 2(a) shows the valence-band photoemission spectra with photon energies in the vicinity of the Ni L_3 white line. The solid (dashed) lines represent spectra with the spin direction of the incident photons parallel (antiparallel) to that of the majority $3d$ electrons. Figure 2(b) shows the differences of the spectra shown in Fig. 2(a)
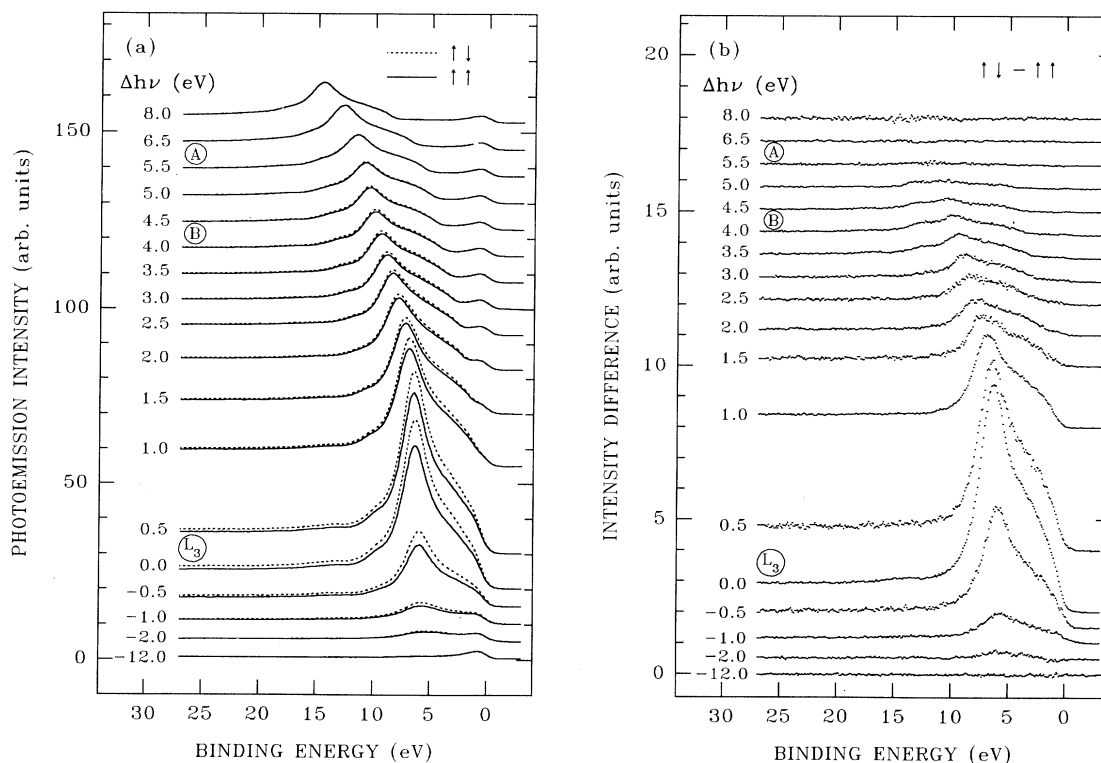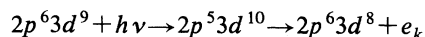

FIG. 2. Valence-band photoemission spectra of Ni taken with photon energies in the vicinity of the Ni L_3 ($2p_{3/2} \rightarrow 3d$) absorption edge: (a) solid (dashed) lines are spectra taken with the spin directions of the photons parallel $\uparrow\uparrow$ (antiparallel $\uparrow\downarrow$) to that of the majority $3d$ electrons; (b) the difference between the antiparallel $\uparrow\downarrow$ and parallel $\uparrow\uparrow$ spectra shown in (a). The photon energies indicated are relative to the Ni L_3 white line at 852.7 eV. A and B indicate the energies of the XAS and MCD fine structures shown in Fig. 1.

taken at the same photon energy (the solid curve subtracted form the dashed curve), i.e., the magnetic-circular polarization dependence of the photoemission intensity. The photon energies selected are indicated relative to the Ni L_3 white at 852.7 eV. The off-resonant spectra are taken at 12 eV below the white line ($\Delta h\nu = -12$ eV), showing a main peak near the Fermi level [see Fig. 2(a)] with nearly no polarization dependence [see Fig. 2(b)]. Raising the photon energy towards the white line, the much discussed 6-eV satellite[7] becomes visible in both the normal [Fig. 2(a)] and difference [Fig. 2(b)] spectra, and its intensity increases, reaching a maximum at the white line ($\Delta h\nu = 0$ eV), and then decreases at higher photon energies. For energies several eV above the white line, the normal and difference spectra are dominated by a $L_3 VV$ Auger-like feature. The resonance in the photoemission intensity at the white line is 80 times larger than the off-resonant signal and 4 times larger than the $L_3 VV$ Auger. For the intensity difference, these numbers are even larger as the off-resonant spectrum shows almost no polarization dependence and the Auger feature looses its polarization dependence at 8 eV above the white line.

The presence of satellites in the valence-band and $2p$ core-level photoemission spectra of Ni, which is similar to the CuO case and which cannot be explained by band theory, suggests the importance of electron correlation effects The fact that the high-energy satellite and not the low-energy main peak of the valence-band photoemission spectra resonates at the L_3 edge, suggests that as far as the high-energy spectroscopy is concerned, a local many-body configuration-interaction scheme, such as that in CuO,[8] can be applied for Ni, where one Ni ion is distinguished as an impurity and is surrounded by $4s$ and neighboring $3d$ orbitals, analogous to a Cu ion and O $2p$ ligands in CuO.[8] The fact that the line shape of the Ni resonance has an atomic-like d^8 multiplet structure, similar to that of the CuO resonance[8] and the $2p_{3/2}$ photoelectron-coincident Auger spectrum of Cu and Ni,[9] strongly indicates that the deexcitation channel consists of a photoabsorption process followed by a nonradiative decay of the type

$$2p^6 3d^9 + h\nu \rightarrow 2p^5 3d^{10} \rightarrow 2p^6 3d^8 + e_k$$

(where e_k denotes the photoelectron), consistent with the results from the $3p$ resonance (spin-resolved) valence-band photoemission on the 6-eV satellite of Ni.[7] These findings give evidence that the white lines observed in the total XAS and MCD spectra, can be assigned to the $2p^5 3d^{10}$ configuration, and that the ground state contains mainly the $3d^9$ configuration. Configuration-interaction calculation within the Anderson impurity framework including atomic multiplet structure give results consistent with these assignments.[10,11]

It is interesting to note that the photoemission intensity difference at the white line resonance is proportional to the dichroism in the photoabsorption intensity, i.e., to the difference in the number of $2p$ core holes created with the two different light polarizations. When normalized to the absorption cross section, the photoemission spectra have only minor line shape differences for the two polarizations, suggesting that the nonradiative decay process is

insensitive to the magnetic state of the intermediate state. Such insensitivity can also be inferred from the fact that whenever the photoabsorption has negligible dichroism, as when the photon energies are 8 eV or higher above the white line, the Auger also has a negligible polarization dependence. A theoretical explanation of these results is given elsewhere.[12] Similar observations have been made in spin-polarized Auger studies of Ni, where the spin-polarized differences are attributed to differences in the spin-dependent cross section for the resonating $2p^6 3d^9 \rightarrow 2p^5 3d^{10}$ electron impact excitation, after which an autoionization decay takes place.[13]

To search for possible photoemission resonances at higher photon energies, e.g., in the vicinity of peaks A or B in Fig. 1, one has to separate the $L_3 VV$ Auger-like intensity from the resonating photoemission spectra. It is important to realize that the Auger line shape depends strongly on the excitation energy,[14] especially for energies near the ionization threshold. In fact, such dependence could give information concerning the states in the core-level x-ray photoemission spectrum. Therefore, when raising the photon energy further away from the white line, one should not only look for spectral changes at given binding energies (photoemission resonances) but also at given kinetic energies (Auger energy dependence). It can be shown that such spectral changes for the unpolarized spectra appear mostly at fixed kinetic energies, because the Auger intensity overwhelms the photoemission spectra [Fig. 2(a)]. It is therefore impossible to identify
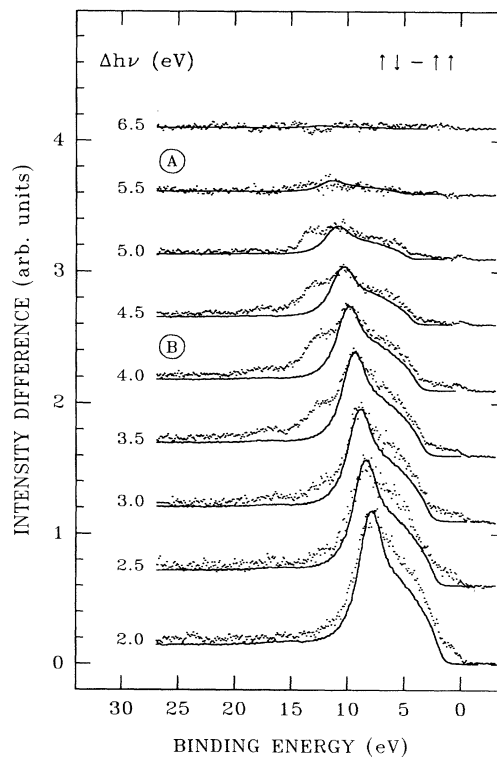

FIG. 3. Comparison between the difference spectra shown in Fig. 2(b) (dots) and the Auger reference spectrum discussed in the text (solid lines). A and B indicate the energies of the XAS and MCD fine structures shown in Fig. 1.

photoemission resonance features in the unpolarized spectra for photon energies several eV above the white line. In the case of the difference spectra [Fig. 2(b)], on the other hand, the Auger intensity is smaller and vanishes rapidly with increasing photon energy, allowing resonance features to become more visible. To facilitate the extraction of the resonance features, we compare the difference spectra with a reference spectrum, which serves as an ansatz for the near ionization threshold Auger spectrum. The obvious choice for this reference is the photoemission difference spectrum at the L_3 white line [Fig. 2(b)], which is almost pure $3d^8$ in character, as discussed above. Figure 3 shows the comparison of the difference spectra with the reference spectrum, which has been shifted to keep the same kinetic energy, and normalized to make the peak heights equal. The results show that the line shapes of the reference spectrum and the difference spectra are essentially the same for photon energies up to 2 eV above the white line, revealing that the Auger spectrum is primarily $3d^8$ in character very close to the ionization threshold. At photon energies near peak B of the MCD spectrum ($\Delta h\nu = 3-5$ eV), a distinct line shape discrepancy can be observed at ≈ 12 eV binding energy. At higher photon energies ($\Delta h\nu > 5.5$ eV), including peak A of the XAS spectrum, the intensities of the difference spectra vanish and, consequently, the line shape discrepancy is negligible. In addition, a small line shape discrepancy can be seen at about 2–8 eV binding energies for the photon energies 2–6 eV above the white line. Line shape discrepancies at given kinetic energies cannot be easily distinguished.

The binding energies of the large line shape discrepancy correspond quite well with that of a $3d^7$-like satellite peak assigned in the photoemission spectrum,[15,16] and its energy separation with $3d^8$-like 6-eV satellite matches that of the $3d^7$- and $3d^8$-like final states observed in the $2p_{3/2}$ photoelectron-coincident Auger of Ni.[9] This strongly suggests that the deexcitation channel in the resonant process involves a photoabsorption and a nonradiative decay process of the type

$$2p^6 3d^8 + h\nu \rightarrow 2p^5 3d^9 \rightarrow 2p^6 3d^7 + e_k \ .$$
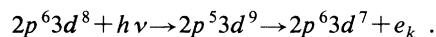
Therefore peak B should be attributed to a $2p^5 3d^9$ configuration in the absorption final state, implying the presence of some $3d^8$ configuration in the ground state. The small line shape discrepancy at 2–8 eV binding energies can be attributed to resonating $3d^8$ photoemission final states, reached via the $2p^5 3d^{10}$ XAS states which are hybridized with the predominant $2p^5 3d^9$ configuration of peak B. Figure 4 summarizes the (net) resonance effects at the L_3 white line an in the vicinity of peak B, where, for the latter, the reference spectrum has been subtracted from the photoemission difference spectrum. Figure 4 also shows the close relationship between the MCD spectrum and the photon energy dependence of the intensities of these valence-band configurations. The results of very recent configuration-interaction calculations[10,11] are in good agreement with both the XAS, MCD, and circularly polarized resonant photoemission data. Depending on the parameters chosen, the $3d^8$, $3d^9$, and $3d^{10}$ weights in the ground state have been calculated to be 21, 61, and
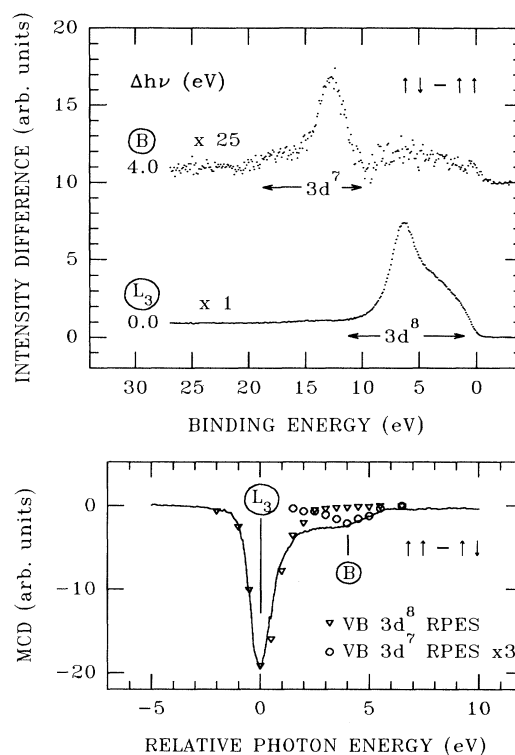

FIG. 4. Upper panel: Magnetic circularly polarized resonant-photoemission spectra at the L_3 white line and at peak B of the MCD spectrum shown in Fig. 1. Lower panel: MCD spectrum together with the photon energy dependence of the intensities of the resonating $3d^8$ (∇) and $3d^7$ (O) valence-band photoemission features.

18% ($\langle n_d \rangle = 8.97$),[10] or 16, 49, and 35% ($\langle n_d \rangle = 9.19$),[11] respectively. In a band-structure picture, where the on-site d-d Coulomb interaction is effectively zero, the weights are different and are given by the broader binomial (statistical) distribution function.[17,18] The ^3F or Hund's rule component is the most important in the $3d^8$ configuration, and the spin and orbital magnetic moments are 0.51 and $0.07\mu_B$,[10] or 0.5 and $0.05\mu_B$,[11] respectively. We note, however, that the Anderson impurity model gives, for peak A, either a XAS intensity too low to account for the measured value, or a MCD intensity so significant that it can be easily detected.[4,5] Within the impurity model, both the A, A' and B, B' peaks belong to the $2p^5 3d^9$ multiplet. Considering the fact that a band-structure analysis[3] gives sufficient XAS intensity without any MCD for peaks A, A', we infer that a large portion of the A, A' intensities should be attributed to a critical point in the band structure. It would be interesting to calculate the spectra, for instance, from an Anderson impurity model which incorporates such critical points or from a multisite cluster model.

In conclusion, we have utilized circularly polarized soft x rays to separate the Auger process from the resonant-photoemission process, and identified the character of the states in the valence-band photoemission spectrum of ferromagnetic Ni. From this we are able to identify the characters of the states in the L_3 x-ray-absorption and magnetic-circular-dichroism spectra, thereby demonstrat-

ing the importance of both electron correlation and band-structure effects in the interpretation of these spectra. Incorporation of both effects in theoretical calculations will be required to understand the electronic structure of transition-metal magnetic compounds, alloys, thin films, and multilayers, where configuration-interaction, atomic multiplet, and band formation effects are comparable. Finally, the experimental results give hope for a combined circular-polarized/spin-polarized soft x-ray resonant-photoemission experiment, which could provide information on the electronic structure of antiferromagnetic and magnetically disordered narrow band materials.

[1] G. Schütz, W. Wanger, W. Wilhelm, P. Kienle, R. Zeller, R. Frahm, and G. Materlik, Phys. Rev. Lett. **58**, 737 (1987); C. T. Chen, F. Sette, Y. Ma, and S. Modesti, Phys. Rev. B **42**, 7262 (1990); L. Baumgarten, C. M. Schneieder, H. Petersen, F. Schäfers, and J. Kirschner, Phys. Rev. Lett. **65**, 492 (1990); T. Koide, T. Shidara, H. Fukutani, K. Yamaguchi, A. Fujimori, and S. Kimura, Phys. Rev. B **44**, 4697 (1991); P. Rudolf, F. Sette, L. H. Tjeng, G. Meigs, and C. T. Chen, J. Magn. Magn. Mater. **109**, 109 (1992); L. H. Tjeng, Y. U. Idzerda, P. Rudolf, F. Sette, and C. T. Chen, *ibid.* **109**, 288 (1992).

[2] B. T. Thole, G. van der Laan, and G. A. Sawatzky, Phys. Rev. Lett. **55**, 2086 (1985); P. Carra and M. Altarelli, *ibid.* **64**, 1286 (1990); T. Jo and S. Imada, J. Phys. Soc. Jpn. **59**, 1421 (1990); G. van der Laan, J. Phys.: Condens. Matter **3**, 1015 (1991); A. Yoshida and T. Jo, J. Phys. Soc. Jpn. **60**, 2098 (1991); B. T. Thole, P. Carra, F. Sette, and G. van der Laan, Phys. Rev. Lett. **68**, 1943 (1992).

[3] C. T. Chen, N. V. Smith, and F. Sette, Phys. Rev. B **43**, 6785 (1991); N. V. Smith, C. T. Chen, F. Sette, and L. F. Mattheiss, *ibid.* **46**, 1023 (1992).

[4] T. Jo and G. Sawatzky, Phys. Rev. B **43**, 8771 (1991).

[5] G. van der Laan and B. T. Thole, J. Phys.: Condens. Matter **4**, 4181 (1992).

[6] C. T. Chen, Nucl. Instrum. Methods Phys. Res. Sect. A **256**, 595 (1987); C. T. Chen and F. Sette, Rev. Sci Instrum. **60**, 1616 (1989); C. T. Chen, *ibid.* **63**, 1229 (1992).

[7] C. Guillot, Y. Ballu, J. Paigné, J. Lecante, K. P. Jain, P. Thiry, R. Pinchaux, Y. Petroff, and L. M. Falikov, Phys. Rev. Lett. **39**, 1632 (1977); D. R. Penn, *ibid.* **42**, 921 (1979); A. Liebsch, *ibid.* **43**, 1431 (1979); M. Iwan, F. J. Himpsel, and D. E. Eastman, *ibid.* **43**, 1829 (1979); L. C. Davis and L. A. Feldkamp,

Phys. Rev. B **23**, 6239 (1981); R. Clauberg, W. Gudat, E. Kisker, E. Kuhlmann, and G. M. Rothberg, Phys. Rev. Lett. **47**, 1314 (1981); Y. Sakisaka, T. Komeda, M. Onchi, H. Kato, S. Masuda, and K. Yagi, *ibid.* **58**, 733 (1987).

[8] L. H. Tjeng, C. T. Chen, J. Ghijsen, P. Rudolf, and F. Sette, Phys. Rev. Lett. **67**, 502 (1991); Y. Seino, H. Ogasawara, A. Kotani, B. T. Thole, and G. van der Laan, J. Phys. Soc. Jpn. **61**, 1859 (1992).

[9] H. W. Haak, G. A. Sawatzky, and T. D. Thomas, Phys. Rev. Lett. **41**, 1825 (1978); G. A. Sawatzky, Treatise Mater. Sci. Technol. **30**, 167 (1988).

[10] A. Tanaka and T. Jo, J. Phys. Soc. Jpn. **61**, 2669 (1992).

[11] We have performed the calculations using parameter values from Ref. 5, which give, in comparison to calculations using values from Refs. 4 and 10, a better agreement for the $2p$ and $3p$ photoemission data. Our magnetic circular polarized $2p$ resonant-photoemission calculations show, however, only minor differences to those reported in Ref. 10.

[12] B. T. Thoel and G. van der Laan (unpublished).

[13] M. Landolt, R. Allenspach, and D. Mauri, J. Appl. Phys. **57**, 3626 (1985).

[14] J. C. Fuggle and G. A. Sawatzky, Phys. Rev. Lett. **66**, 966 (1991).

[15] W. Eberhardt and E. W. Plummer, Phys. Rev. B **21**, 3245 (1983).

[16] O. Björneholm, J. N. Andersen, C. Wigren, A. Nilsson, R. Nyholm, and N. Mårtensson, Phys. Rev. B **41**, 10 408 (1990).

[17] J. Hubbard, Proc. R. Soc. London, Sect. A **276**, 238 (1963).

[18] The statistical $3d^6$, $3d^7$, $3d^8$, $3d^9$, and $3d^{10}$ weights are 1.2, 6.1, 20, 39, and 34 % ($\langle n_d \rangle = 8.97$) and 0.5, 3.5, 15, 38, and 43 % ($\langle n_d \rangle = 9.19$).